ELSEVIER

Biochimica et Biophysica Acta 1513 (2001) 55–62

BIOCHIMICA ET BIOPHYSICA ACTA
BBA

www.bba-direct.com

Imaging mixed lipid monolayers by dynamic atomic force microscopy

Magali Deleu [a], Katherine Nott [a], Robert Brasseur [b], Philippe Jacques [c], Philippe Thonart [d], Yves F. Dufrêne [e,*]

[a] *Unité de Chimie Biologique Industrielle, Faculté Universitaire des Sciences Agronomiques de Gembloux, Passage des Déportés, 2, B-5030 Gembloux, Belgium*

[b] *Centre de Biophysique Moléculaire Numérique, Faculté Universitaire des Sciences Agronomiques de Gembloux, Passage des Déportés, 2, B-5030 Gembloux, Belgium*

[c] *Unité de Bio-industries, Faculté Universitaire des Sciences Agronomiques de Gembloux, Passage des Déportés, 2, B-5030 Gembloux, Belgium*

[d] *Centre Wallon de Biologie Industrielle, Université de Liège, 4000 Liège, Belgium*

[e] *Unité de Chimie des Interfaces, Université Catholique de Louvain, Place Croix du Sud 2/18, 1348 Louvain-la-Neuve, Belgium*

Received 1 February 2001; received in revised form 3 April 2001; accepted 11 April 2001

Abstract

Phase imaging with tapping mode atomic force microscopy (AFM) and force modulation microscopy were used to probe the mechanical properties of phase-separated lipid monolayers made of a mixture (0.25:0.75) of the surface-active lipopeptide surfactin and of dipalmitoylphosphatidylcholine (DPPC). The π–A isotherms and the result of a molecular modeling study revealed a loose, 2-D liquid-like organization for the surfactin molecules and a closely packed, 2-D solid-like organization for DPPC molecules. This difference in molecular organization was responsible for a significant contrast in height, tapping mode phase and force modulation amplitude images. Phase imaging at light tapping, i.e., with a ratio of the set-point tapping amplitude with respect to the free amplitude $A_{sp}/A_0 \approx 0.9$, showed larger phase shifts on the solid-like DPPC domains attributed to larger Young's modulus. However, contrast inversion was observed for $A_{sp}/A_0 < 0.7$, suggesting that at moderate and hard tapping the image contrast was dominated by the probe–sample contact area. Surprisingly, force modulation amplitude images showed larger stiffness for the liquid-like surfactin domains, suggesting that the contrast was dominated by contact area effects rather than by Young's modulus. These data emphasize the complex nature of the contrast mechanisms of dynamic AFM images recorded on mixed lipid monolayers.

Keywords: Atomic force microscopy; Force modulation; Lipid monolayer; Nanometer scale; Tapping mode

1. Introduction

Atomic force microscopy (AFM) has become a well-established technique in biochemistry and biophysics to characterize supported lipid films (for a review, see [1]). It can be used to characterize the molecular structure of lipid films [2], the formation of structural defects [3], the effect of external agents on film structure [4] and the organization of phase-separated films [5–8]. Besides the widely used static contact mode, more recent dynamic imaging modes now offer the possibility of probing nanomechanical

* Corresponding author. Fax: +32-10-47-20-05; E-mail: dufrene@cifa.ucl.ac.be

0005-2736/01/$ – see front matter
PII: S0005-2736(01)00337-6

properties. In tapping mode atomic force microscopy (TMAFM), the probe is excited externally and the amplitude and phase of the cantilever are monitored near the resonance frequency of the cantilever. Phase imaging with TMAFM, which is based on detecting the phase lag of the cantilever oscillation relative to the signal sent to the piezo driver of the cantilever, has proved useful to elucidate variations in material properties such as adhesion, friction and viscoelasticity [9–13]. Czajkowsky et al. [6] used TMAFM in the phase shift mode to directly visualize phase-separated lipid bilayers with different surface charge characteristics. Force modulation microscopy (FMM) is another dynamic mode which measures the amplitude and phase shift of the cantilever while the sample or the probe is vibrated, thereby allowing to probe spatial variations of viscoelasticity [14–18]. While phase imaging and FMM have been widely used to characterize polymeric materials [10–13,16,18], applications dealing with lipid films are scarce [6]. Such measurements are of great potential interest in biophysics, e.g. for gaining insight into the nanomechanics of biomembranes.

Surfactin (Fig. 1) is a lipopeptide produced by various *Bacillus subtilis* strains which exhibits strong surface activity and important biological properties [19]. The interactions of surfactin with biological membranes are known to determine its biological activity and involve insertion into the lipid bilayers, permeability changes and membrane disruption [20,21]. Hence, there is a substantial interest in understanding the molecular organization and nanomechanical properties of mixed surfactin/lipid films. In a previous study [22], static contact mode AFM was used in combination with X-ray photoelectron spectroscopy (XPS) to investigate mixed monolayers of surfactin and of dipalmitoylphosphatidylcholine (DPPC). Height images of mixed monolayers showed phase separation, the step height measured between the lower surfactin domains and the higher DPPC domains being 1.2 ± 0.1 nm. Here, we use phase imaging and FMM to probe the film nanomechanical properties and gain insight into the contrast mechanisms of dynamic AFM images. Interpretation of the images is supported by a molecular modeling study of mixed monolayers at a hydrophobic/hydrophilic interface.

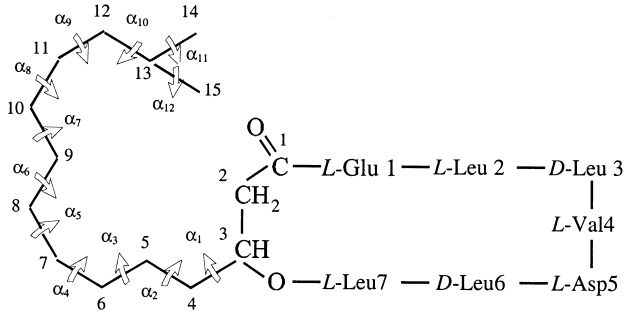

Fig. 1. Primary structure of surfactin showing the numbering of the carbon atoms of the β-hydroxy fatty acid side chain and the torsional angles (α_i).

2. Materials and methods

Surfactin with a β-hydroxy fatty acid chain of 15 carbon atoms (MW: 1036) was used in this study. It was produced and purified as described previously [23]. Primary structure and purity of the surfactin-C_{15} (>95%) were ascertained by analytical RP-HPLC (Chromspher 5 μm C18 column, 1×25 cm, Chrompack, Middelburg, The Netherlands), amino acid analysis, and electrospray mass spectrometry (Finnigan MAT 900 ST) measurements.

LB monolayers were prepared at 20°C with an automated LB system (LFW2 3″5, Lauda, Königshofen, Germany). Surfactin and DPPC purchased from Sigma (St. Louis, MO, USA) were dissolved at 1 mM in chloroform/methanol (2:1). Pure solutions and (0.25:0.75) molar mixtures of surfactin and DPPC were spread on a milliQ water (Millipore, Milford, MA, USA) subphase adjusted at pH 2.0. After evaporation of the solvent, monolayers were compressed at a rate of 150 cm^2/min. They were deposited at a constant surface pressure of 20 mN/m, i.e., well below the collapse pressure, by raising vertically freshly cleaved mica through the air–water interface at a rate of 10 mm/min. The transfer ratios were all close to 1:1. This procedure yielded supported monolayers in which the polar head groups are in contact with the mica surface and the alkyl chains exposed to the air. For determining the compression isotherm curves, films were compressed at a rate of 61.8 cm^2/min. The difference between molecular areas of two independent sets of measurements was less than 2.5%.

Theoretical analysis of the organization of a surfactin molecule embedded in a DPPC matrix was

performed using a semi-empirical method [24]. In a first step, the conformation and the orientation of a surfactin molecule were analyzed at a hydrophobic/hydrophilic interface. The atomic coordinates of the surfactin ring structure provided by Bonmatin et al. [25] were used as a starting point. Twelve carbon atoms were added to the methyl moiety outside of the ring using the Hyperchem 5.0 software (Autodesk, Sausalito, USA) to complete the β-hydroxy fatty acid chain. The total conformational energy that represents the sum of the van der Waals interactions, the torsional potential and the electrostatic interactions was calculated for a large number of surfactin conformations in a systematic analysis bearing on all torsional angles (α) (Fig. 1). Those angles were affected by systematic 60° changes using two successive analyses. The first one was performed on angles α_1 to α_6 generating 46 656 (6^6) conformations. The second analysis was performed on angles from α_5 to α_9 generating 7776 (6^5) conformations. In total, 54 432 conformations were generated. Conformations with probabilities of existence $< 5\%$ were discarded. Selected conformations were then submitted to a simplex minimization procedure [26]. This calculation was carried out in a medium of intermediate dielectric constant of a hydrophobic/hydrophilic interface. The most probable conformation based on a Boltzmann statistical weight was selected and its orientation at the hydrophobic/hydrophilic interface was defined by calculations of the hydrophobic and hydrophilic centers as described elsewhere [24]. In the second step, the conformation of a surfactin molecule embedded in a DPPC matrix was established using the hypermatrix procedure from Tammo (Theoretical Analysis of Molecular Membrane Organization) software as detailed elsewhere [27]. The position of the central surfactin molecule was fixed and two layers of DPPC molecules were added one by one around it in order to maintain a minimal energy. Molecule visualization was performed using WinMGM software [28] from Ab Initio Technology (Obernai, France).

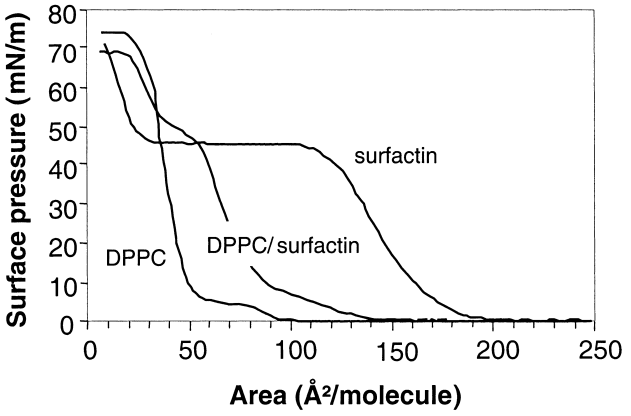

Fig. 2. Surface pressure–area (π–A) isotherms, at the air–water interface, of pure surfactin and DPPC monolayers and of mixed (0.25:0.75) surfactin/DPPC monolayers recorded at 20°C with a water subphase at pH 2.0.

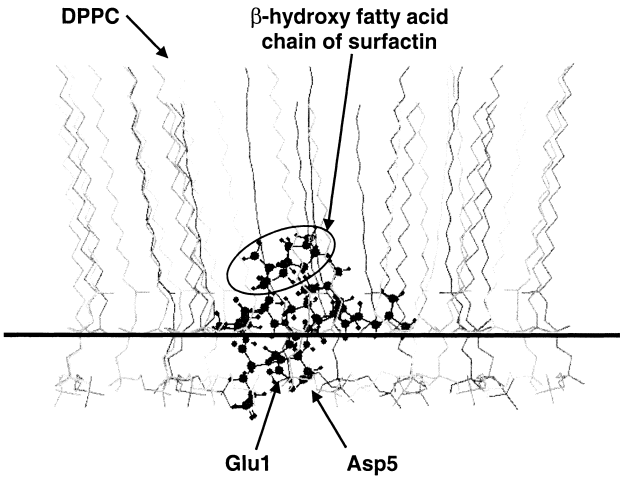

Fig. 3. Molecular model of a surfactin molecule embedded in a DPPC matrix at a hydrophobic/hydrophilic interface (horizontal line). The hydrophilic medium is located under the interface. The two acidic chains of the Asp and Glu residues and the β-hydroxy fatty acid chain of the surfactin are showed in the figure.

AFM measurements were performed in air at room temperature (20°C) using a commercial optical lever microscope (Nanoscope III, Digital Instruments, Santa Barbara, CA, USA). Scan rates were typically in the range of 1–2 Hz. FMM imaging was performed using oxide-sharpened microfabricated Si_3N_4 cantilevers (Park Scientific Instruments, Mountain View, CA, USA) with typical radius of curvature of 20 nm and spring constants ranging from 0.01 N/m to 0.5 N/m. The imaging force was kept as low as possible (≤1 nN). The cantilever was vibrated using a piezoelectric actuator driven at its resonant frequency, i.e. approx. 7.2 kHz. Integral and proportional gains of the feedback loop were typically equal to 7 and 8, respectively. The driving amplitude was varied from 50 mV to 400 mV. TMAFM was performed using silicon cantilevers

(Nanosensors, Aidlingen, Germany) with a resonance frequency of 280–300 kHz and a spring constant of 21–78 N/m. Integral and proportional gains of the feedback loop were typically equal to 0.2 and 2, respectively. The cantilever was vibrated slightly below its resonant frequency. Driving amplitudes of 100 mV and 200 mV were tested and the ratio of the amplitude of the set-point oscillation to the free oscillation was varied from 0.9 to 0.1.

3. Results and discussion

The surface pressure–area (π–A) isotherms, at the air–water interface, of pure surfactin and DPPC monolayers, and of mixed surfactin/DPPC monolayers at 0.25 surfactin molar ratio are presented in Fig. 2. At 20 mN/m, DPPC and surfactin occupy 46 and 142 Å^2/molecule, respectively. The shape of the isotherms indicates that, at 20 mN/m, the DPPC monolayer is characterized by a 2-D solid-like organization, while surfactin has a 2-D liquid-like organization. The area of DPPC at 20 mN/m reflects a vertical, or slightly tilted, orientation of the lipid molecules [29]. In contrast, the large area of surfactin would correspond to an orientation in which the peptide ring is lying horizontally [30]. At higher surface pressure, the surfactin isotherm shows a horizontal plateau. Then, a sharp increase of surface pressure is observed at very low areas per molecule, reflecting a condensed state in which the peptide rings are probably perpendicular to the interface [31].

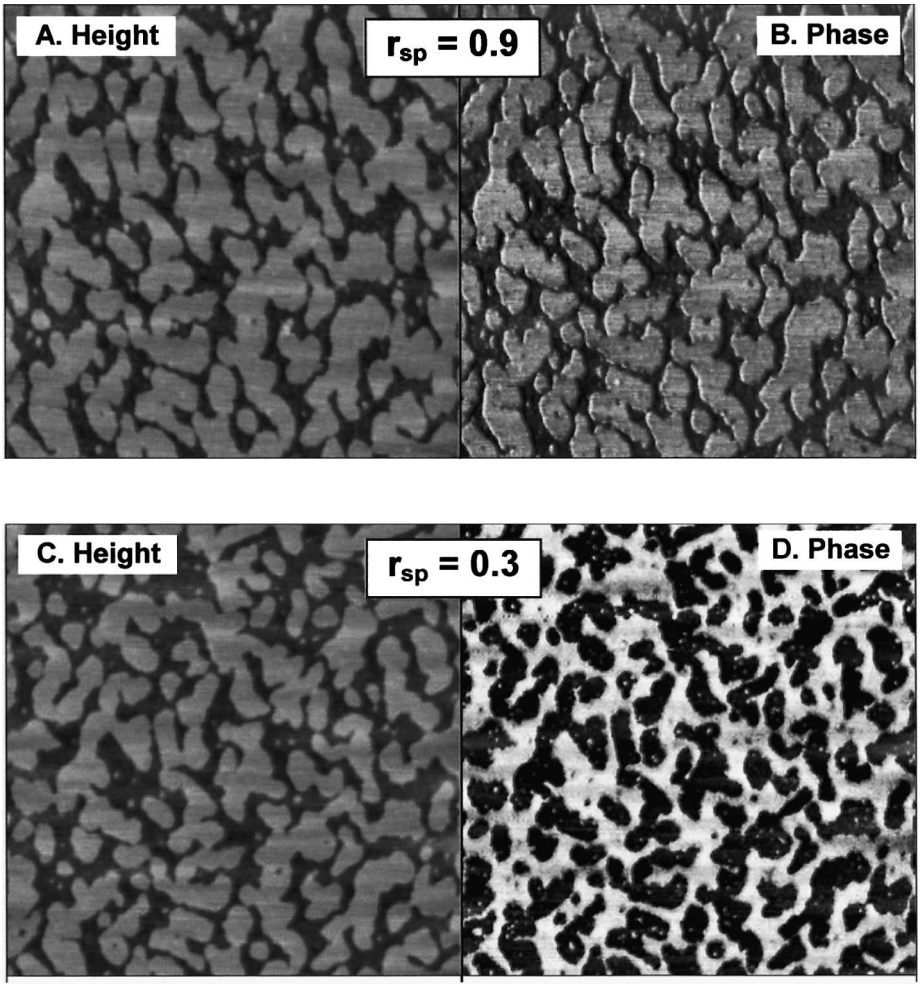

Fig. 4. Tapping mode height (A,C) and phase (B,D) images (2 μm×2 μm) of a mixed surfactin/DPPC monolayer in air recorded at r_{sp} = 0.9 (A,B) and r_{sp} = 0.3 (C,D). z-range: 10 nm (A,C), 5° (B) and 25° (D).

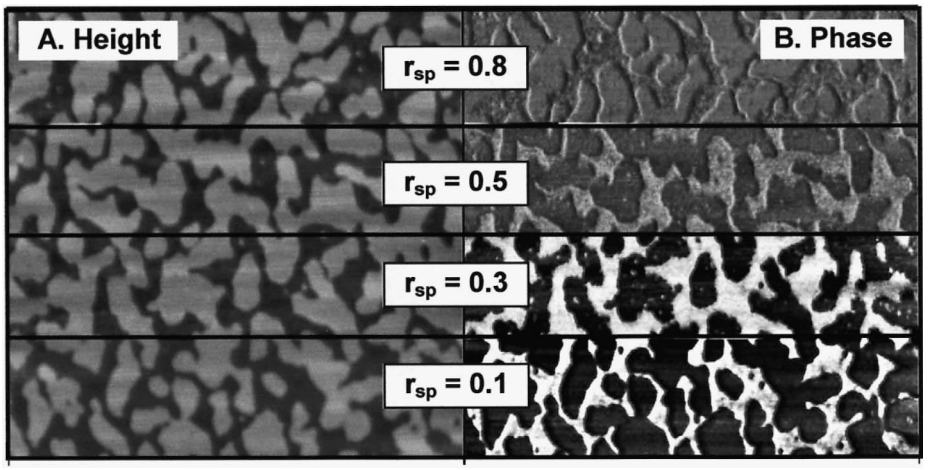

Fig. 5. Tapping mode height (A) and phase (B) images (2 μm×2 μm) of a mixed surfactin/DPPC monolayer recorded while decreasing the r_{sp} ratio. *z*-range: 10 nm (A) and 20° (B).

To gain further insight into the monolayer organization, a theoretical analysis at a hydrophobic/hydrophilic interface was performed. Fig. 3 presents the most probable computational model of a surfactin molecule embedded in a DPPC matrix. In this model, the peptide ring of the surfactin is positioned in the plane of the interface with the two acidic chains close to each other and protruding in the hydrophilic medium and the β-hydroxy fatty acid chain folded on top of the ring. By contrast, the DPPC molecules are closely packed with their alkyl chains almost vertically oriented. This gives rise to a height difference between the two molecules of 1.33 nm.

Dynamic AFM imaging was performed on mixed surfactin/DPPC monolayers supported on mica with the aim to better understand the film mechanical properties. Tapping mode was conducted while varying the set-point amplitude ratio r_{sp}, i.e. the ratio of the amplitude of the set-point oscillation to the free oscillation. Fig. 4 shows height and phase images recorded at two r_{sp} ratios, i.e. 0.9 and 0.3 (driving amplitude of 200 mV, corresponding to an actual oscillation amplitude of approx. 75 nm). The height images are not significantly affected by changes in the r_{sp} ratio. They reveal phase separation for the mixed surfactin/DPPC monolayer, the height difference between the two domains being 1.2 ± 0.1 nm, which is in accordance with the step height deduced from the theoretical analysis and with the height difference measured in contact mode AFM images [22]. Previous characterization of mixed monolayers prepared at different surfactin molar ratios by contact mode AFM and XPS [22] revealed that: (i) the lower and higher levels in the AFM topographic images can be unambiguously assigned to surfactin and DPPC, respectively; (ii) surfactin and DPPC are completely immiscible in the conditions investigated; (iii) the measured step height results from a difference in molecular orientation.

Strikingly, the phase images show a contrast inversion on decreasing the r_{sp} ratio: the 2-D solid-like DPPC domains show larger phase shifts than the 2-D liquid-like surfactin domains at $r_{sp} = 0.9$ (approx. 0.5° higher phase shift), while the opposite is observed at $r_{sp} = 0.3$ (approx. 6.5° smaller phase shift). Fig. 5 shows height and phase images recorded while progressively decreasing the r_{sp} ratio. Contrast inversion occurs at $r_{sp} \approx 0.7$ and below that value, the contrast increases with decreasing r_{sp}. Similar trends were observed at a driving amplitude of 100 mV, except that the contrast was less pronounced, while amplitudes smaller than 100 mV failed to give satisfactory, reproducible results. This suggests that at small amplitudes, the response is strongly influenced by the surface contamination layer [10] and emphasizes the need to operate at sufficiently high amplitudes in order to be sensitive to sample–probe interactions.

The question of the physical origin of the phase shift is a complex issue. However, assuming that phase shift images reported here essentially measure the energy dissipation associated with the intermit-

tent contact between probe and sample [13], an explanation may be proposed to account for the contrast inversion. Previous work on polymeric materials [10] has shown that the phase image contrast depends on the r_{sp} ratio and on the free oscillation amplitude A_0, the effective probe–sample force increasing with decreasing r_{sp} and increasing A_0. Our observation of a larger contrast upon decreasing r_{sp} and increasing A_0 is thus consistent with these data. To account for the contrast inversion, it is necessary to recall that the surface stiffness S increases with the effective modulus of the probe–sample contact E^* and with the contact area A according to:

$$\langle S\rangle \propto \langle A\rangle^{1/2}\, E^* \quad (1)$$

Since in tapping mode, the probe–sample contact area varies with time during each contact, it is appropriate to use time-averaged values of the contact area and surface stiffness over one cycle of oscillation, i.e. $\langle A\rangle$ and $\langle S\rangle$ [10]. Eq. 1 indicates that the stiffness $\langle S\rangle$ is proportional to E^*, which is dominated by the modulus of the sample when the probe is harder than the sample. However, the stiffness is also proportional to $\langle A\rangle^{1/2}$ and a softer material leads to a larger contact area. Hence, the stiffness may be larger on a region of smaller Young's modulus if it is dominated by the contact area. This behavior has been observed experimentally [10]: at light and moderate tapping, the phase contrast of polymeric samples was shown to result from differences in adhesion and sample stiffness, respectively, while at hard tapping, the contrast was inverted and dominated by contact area. This leads us to suggest that the contrast inversion observed at moderate ($A_{sp}/A_0 \approx 0.5$) and hard ($A_{sp}/A_0 \approx 0.2$) tapping on the mixed monolayers results from probe–sample contact area effects. The above discussion is purely qualitative since the relationship between the changes in the A_{sp}/A_0 ratios and the film indentation depth is not known. To gain quantitative information, it would be most interesting in future studies to perform approach curves which give the variations of the amplitude and phase as a function of the indentation depth. Another important issue would be to assess the possible influence of the A_{sp}/A_0 ratio on the lateral resolution of height images. One may anticipate that contact area effects at low A_{sp}/A_0 ratios will decrease the resolution.

Force modulation microscopy probes the relative stiffness by recording variations in the amplitude of the probe deflection across the surface, stiffer areas resulting in a higher deflection amplitude. It is important to realize that the microscope software is configured so that a region of higher amplitude in the amplitude image appears darker. Fig. 6 shows height and amplitude images recorded for a mixed surfactin/DPPC monolayer (driving amplitude of 100 mV). The image contrast increases with driving amplitude as illustrated in Fig. 7. Strikingly, the amplitude image indicates a larger stiffness (approx. 0.06 nm higher amplitude) for 2-D liquid-like surfactin domains than for 2-D solid-like DPPC. The contrast mechanism may tentatively be understood within the same framework as the one developed for phase imaging (Eq. 1). The unexpected contrast would thus be due to the influence of probe–sample

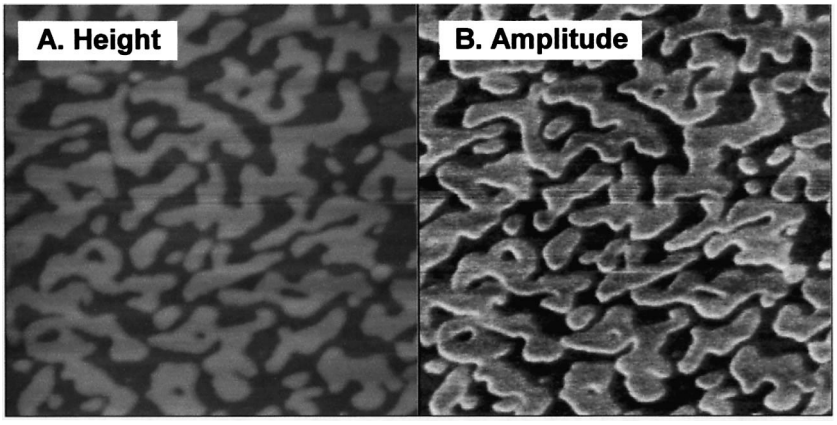

Fig. 6. Force modulation height (A) and amplitude (B) images (2 μm×2 μm) of a mixed surfactin/DPPC monolayer. z-range: 20 nm (A) and 0.5 nm (B).

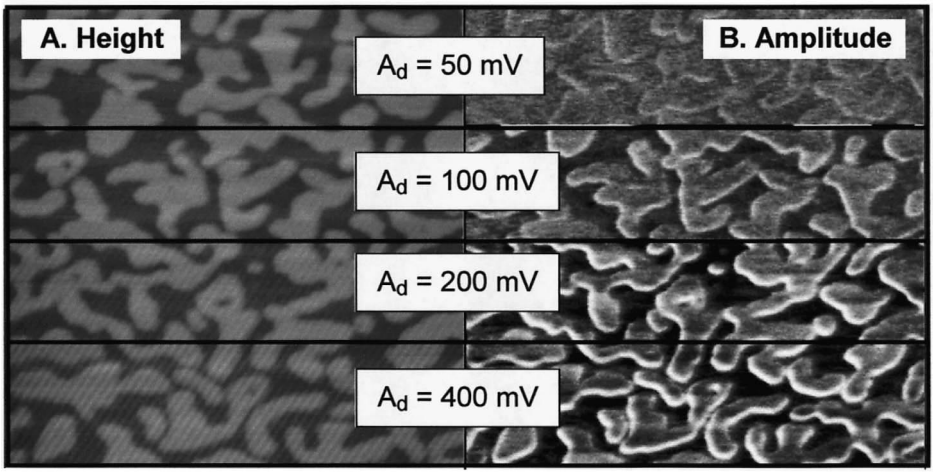

Fig. 7. Height (A) and amplitude (B) images (2 μm×2 μm) of a mixed surfactin/DPPC monolayer recorded while increasing the driving amplitude A_d. z-range: 20 nm (A) and 0.5 nm (B).

contact area. These results, similar to those reported for patterned alkanethiol monolayers on gold [15], suggest that for lipid monolayers FMM may probe variations of contact area rather than of Young's modulus.

To conclude, the results emphasize the complex nature of the contrast mechanisms of dynamic AFM images recorded on lipid monolayers. Molecular modeling reveals a loose organization for the surfactin molecule and a closely packed organization for DPPC, in agreement with the π–A isotherms. This difference in molecular organization gives rise to significant contrast in both tapping mode phase and force modulation amplitude images. The image contrast is highly dependent on the r_{sp} ratio and driving amplitude, respectively.

Acknowledgements

The support of the National Foundation for Scientific Research (FNRS) and of the Federal Office for Scientific, Technical and Cultural Affairs (Interuniversity Poles of Attraction Programme) is gratefully acknowledged. M.D. thanks the FNRS for her position as Research Assistant. The authors thank P. Grange for the use of the atomic force microscope, O. Bouffioux for preparing the molecular model image, M. Paquot, V. De Cupere and B. Nysten for valuable discussions and A. Nott for critical reading of the paper.

References

[1] Y.F. Dufrêne, G. U Lee, Biochim. Biophys. Acta 1509 (2000) 14–41.
[2] J.A.N. Zasadzinski, C.A. Helm, M.L. Longo, A.L. Weisenhorn, S.A.C. Gould, P.K. Hansma, Biophys. J. 59 (1991) 755–760.
[3] Y. Fang, J. Yang, Biochim. Biophys. Acta 1324 (1997) 309–319.
[4] J. Mou, J. Yang, C. Huang, Z. Shao, Biochemistry 33 (1994) 9981–9985.
[5] Y.F. Dufrêne, W.R. Barger, J.-B.D. Green, G.U. Lee, Langmuir 13 (1997) 4779–4784.
[6] D.M. Czajkowsky, M.J. Allen, V. Elings, Z. Shao, Ultramicroscopy 74 (1998) 1–5.
[7] V. Vié, N. Van Mau, E. Lesniewska, J.P. Goudonnet, F. Heitz, C. Le Grimellec, Langmuir 14 (1998) 4574–4583.
[8] I. Reviakine, A. Simon, A. Brisson, Langmuir 16 (2000) 1473–1477.
[9] Q. Zong, D. Innis, K. Kjoller, V.B. Elings, Surf. Sci. Lett. 290 (1993) L688–L692.
[10] S.N. Magonov, V. Elings, M.-H. Whangbo, Surf. Sci. Lett. 375 (1997) L385–L391.
[11] G. Bar, R. Brandsch, M.-H. Whangbo, Langmuir 14 (1998) 7343–7347.
[12] G. Bar, Y. Thomann, M.-H. Whangbo, Langmuir 14 (1998) 1219–1226.
[13] B.D. Beake, J.S.G. Ling, G.J. Leggett, Polymer 41 (2000) 2241–2248.
[14] M. Radmacher, R.W. Tillmann, H.E. Gaub, Biophys. J. 64 (1993) 735–742.
[15] G. Bar, S. Rubin, A.N. Parikh, B.I. Swanson, T.A. Zawodzinski Jr., M.-H. Whangbo, Langmuir 13 (1997) 373–377.
[16] E. Tomasetti, R. Legras, B. Nysten, Nanotechnology 9 (1998) 305–315.

[17] L.F. Chi, M. Gleiche, H. Fuchs, Langmuir 14 (1998) 875–879.
[18] B.D. Beake, G.J. Leggett, P.H. Shipway, Surf. Interface Anal. 27 (1999) 1084–1091.
[19] A. Kakinuma, A. Ouchida, T. Shima, H. Sugino, H. Isono, G. Tamura, K. Arima, Agric. Biol. Chem. 33 (1969) 1669–1671.
[20] J.D. Sheppard, C. Jumarie, D.G. Cooper, R. Laprade, Biochim. Biophys. Acta 1064 (1991) 13–23.
[21] R. Maget-Dana, M. Ptak, Biophys. J. 68 (1995) 1937–1943.
[22] M. Deleu, M. Paquot, P. Jacques, P. Thonart, Y. Adriaensen, Y.F. Dufrêne, Biophys. J. 77 (1999) 2304–2310.
[23] H. Razafindralambo, Y. Popineau, M. Deleu, C. Hbid, P. Jacques, P. Thonart, M. Paquot, J. Agric. Food Chem. 46 (1998) 911–916.
[24] R. Brasseur, J.M. Ruysschaert, Biochem. J. 238 (1986) 1–11.
[25] J.M. Bonmatin, M. Genest, H. Labbé, M. Ptak, Biopolymers 37 (1994) 975–986.
[26] J.A. Nelder, R. Mead, Comput. J. 7 (1965) 308.
[27] R. Brasseur, J.A. Killian, B. De Kruijff, J.M. Ruysschaert, Biochim. Biophys. Acta 903 (1987) 11–17.
[28] M. Rahman, R. Brasseur, J. Mol. Graph. 12 (1994) 212–218.
[29] J. Marra, J. Israelachvili, Biochemistry 24 (1985) 4608–4618.
[30] X. Gallet, M. Deleu, H. Razafindralambo, P. Jacques, P. Thonart, M. Paquot, R. Brasseur, Langmuir 15 (1999) 2409–2413.
[31] R. Maget-Dana, M. Ptak, J. Colloid Interface Sci. 153 (1992) 285–291.